Hyperbolic Numerics for Variational Approaches to Correspondence Problems

Henning Zimmer[1,2], Michael Breuß[1], Joachim Weickert[1], and Hans-Peter Seidel[2]

[1] Mathematical Image Analysis Group,
Faculty of Mathematics and Computer Science,
Building E1.1, Saarland University, 66041, Saarbrücken, Germany
{zimmer,breuss,weickert}@mia.uni-saarland.de
[2] Max-Planck Institute for Informatics,
Stuhlsatzenhausweg 85, 66123 Saarbrücken, Germany
hpseidel@mpi-sb.mpg.de

Abstract. Variational approaches to correspondence problems such as stereo or optic flow have now been studied for more than 20 years. Nevertheless, only little attention has been paid to a subtle numerical approximation of derivatives. In the area of numerics for hyperbolic partial differential equations (HDEs) it is, however, well-known that such issues can be crucial for obtaining favourable results. In this paper we show that the use of hyperbolic numerics for variational approaches can lead to a significant quality gain in computational results. This improvement can be of the same order as obtained by introducing better models. Applying our novel scheme within existing variational models for stereo reconstruction and optic flow, we show that this approach can be beneficial for all variational approaches to correspondence problems.

1 Introduction

Numerous tasks in the field of computer vision belong to the class of *correspondence problems*, where one has to match pixels of two or more images. Popular examples are stereo reconstruction and optic flow, that both amount to computing a displacement field between two images. In the stereo context, the absolute value of this field is called *disparity* and is needed to recover the depth information of a static scene. For optic flow, the displacement field is called *optic flow field* and gives information about the dynamics of a moving scene.

A successful class of techniques for solving correspondence problems like stereo or optic flow are the *variational approaches* that find the displacement field as the minimiser of a continuous energy functional. Those methods have been studied for more than two decades, starting from the optic flow approach of Horn and Schunck [1]. During this period of time, lots of effort has been spent to improve the quality of models [2, 3, 4, 5, 6, 7].

In order to apply those continuous models to sampled digital images and for solving the minimisation problem on a computer, one certainly has to *discretise*

X.-C. Tai et al. (Eds.): SSVM 2009, LNCS 5567, pp. 636–647, 2009.
© Springer-Verlag Berlin Heidelberg 2009

occurring image derivatives. This task obviously offers a certain degree of freedom in choosing a well-suited derivative approximation. Surprisingly, this issue has hardly been studied for variational approaches to correspondence problems. If the discretisation is discussed at all, most approaches use "standard" central finite difference approximations [3, 4, 5].

For variational approaches to image restoration, sophisticated approximation schemes have already been considered for a long time [8, 9]. They also have been thoroughly studied in the field of *hyperbolic partial differential equations (HDEs)* [10, 11], where one simulates the transport of liquids or gases, resulting in a problem setting related to correspondence problems: Given an initial density distribution (first image) and the velocity of transport (displacement), compute the density distributions at later times (second image). One realises that the role of known and unknown is switched compared to correspondence problems.

In this paper we make use of this relation between HDEs and correspondence problems for the first time in the literature. In the style of numerical schemes for HDEs, we develop an adaptive discretisation scheme that decides, based on a smoothness measure, on a suitable approximation of image derivatives at each point. This scheme is then used within variational frameworks for stereo reconstruction and optic flow. Experiments show that this approach improves the quality of results in the same order as can be achieved with model refinements.

This paper is organised as follows: In Sect. 2 we investigate the importance of an appropriate approximation of image derivatives on the example of simple 1-D correspondence problems. Based on this we develop the adaptive discretisation scheme that is applied to stereo reconstruction and optic flow in Sect. 3 and Sect. 4, respectively. There we also show corresponding experiments. The paper is then concluded by a summary and an outlook on future work in Sect. 5.

2 Hyperbolic Numerics for 1-D Variational Approaches

2.1 A Variational Approach for 1-D Correspondence Problems

For simplicity, let us consider a 1-D signal sequence $f(x,t)$ where $x \in \Omega$ denotes the position in the signal domain $\Omega \subset \mathbb{R}$ and $t \geq 0$ denotes time. In order to compute the unknown displacement function $u(x)$ that gives the displacements from time t to $t+1$, we minimise the energy functional

$$E(u) = \int_{\Omega} \Big[(f_x\, u + f_t)^2 + \alpha\, u_x^2 \Big] \, \mathrm{d}x \ , \tag{1}$$

where subscripts denote partial derivatives.

The term $(f_x\, u + f_t)^2$ is called *data term* and models how well the displacement u matches the signal sequence f. We impose that the signal values are invariant under their displacement, i.e., $f(x+u, t+1) = f(x,t)$. Assuming that u is small and f sufficiently smooth, we can perform a linearisation that finally leads to the presented data term. Note that in the 1-D setting, the data term alone allows to compute a solution $u = -f_t/f_x$, if $f_x \neq 0$. However, in 2-D this will no longer be the case.

There, and also to obtain a solution in flat signal regions, the *smoothness term* u_x^2 is needed. By penalising large derivatives of u, it allows to smoothly fill in the displacement function where the data term is not sufficient. Its contribution to the energy is steered by a smoothness weight $\alpha > 0$.

In order to actually compute a minimiser u of the energy (1), the calculus of variations states that u necessarily has to fulfil the *Euler-Lagrange equation*

$$f_x\,(f_x\,u + f_t) - \alpha\,u_{xx} = 0 \quad , \tag{2}$$

with homogeneous Neumann boundary conditions.

2.2 A Closer Look into Discretisation Issues

For solving the Euler-Lagrange equation (2) on a computer, we have to discretise the signal f, the displacement u and their derivatives f_x, f_t and u_{xx}. Note that the image derivatives that occur in the Euler-Lagrange equation (2) are in general the same as in the linearised data term of the energy (1). Thus, the data term suffices to find out which derivatives have to be approximated.

Let us start with the discretisation of the signals f and u. To this end we sample them on a spatio-temporal *discrete grid* which yields the approximations $f(x_i, t_k) \approx f_i^k$ and $u(x_i) \approx u_i$ where $x_i := (i - \frac{1}{2})\,h$ and $t_k = k\,\tau$ for a spatial grid size h and a time step size τ. In this paper we will only consider the two frames f_i^k and f_i^{k+1}, assuming a temporal sampling of $\tau = 1$.

Derivative Approximations. The discretisation of the occurring derivatives can be done in different ways. We use the popular concept of *finite differences*, as for example presented in [12]. As notation for the approximation of partial derivatives we use $f_d(x_i, t_k) \approx (f_d)_i^k$ to denote the corresponding finite difference discretisation.

I. Temporal Discretisation. For the time derivative we use the forward difference

$$(f_t)_i^k := \frac{1}{\tau}\left(f_i^{k+1} - f_i^k\right) \quad , \tag{3}$$

as this is the only reasonable choice, given f_i^k and f_i^{k+1}.

II. Spatial Discretisation of First Order. The approximation of f_x offers different possibilities for $(f_x)_i^k$. Basic choices are *forward*, *backward* and *central* differences:

$$\begin{aligned}
\mathcal{D}_x^+ f_i^k &:= \frac{1}{h}\left(f_{i+1}^k - f_i^k\right), & \mathcal{D}_x^+ f_i^{k+1} &:= \frac{1}{h}\left(f_{i+1}^{k+1} - f_i^{k+1}\right) \quad , \\
\mathcal{D}_x^- f_i^k &:= \frac{1}{h}\left(f_i^k - f_{i-1}^k\right), & \mathcal{D}_x^- f_i^{k+1} &:= \frac{1}{h}\left(f_i^{k+1} - f_{i-1}^{k+1}\right) \quad , \\
\mathcal{D}_x^0 f_i^k &:= \frac{1}{2h}\left(f_{i+1}^k - f_{i-1}^k\right), & \mathcal{D}_x^0 f_i^{k+1} &:= \frac{1}{2h}\left(f_{i+1}^{k+1} - f_{i-1}^{k+1}\right) \quad ,
\end{aligned} \tag{4}$$

where $\mathcal{D}^+$ denotes forward, $\mathcal{D}^-$ backward and $\mathcal{D}^0$ central differences, respectively, that can be computed at the time level k or $k+1$.

Note that the approximation error of the *one-sided differences* (forward and backward) is in $\mathcal{O}(h)$, whereas their central counterparts only involve an error of $\mathcal{O}(h^2)$. This, together with the unbiased stencil orientation, explains why they are a popular "standard" choice in image processing applications. To further reduce the approximation error one may consider *averaged differences*, taking into account the time level k and $k+1$. In the remainder of this paper those will be referred to as "standard" derivative approximation. They are given by

$$\mathcal{D}_x^0 f_i^{k+\frac{1}{2}} := \frac{1}{2}\left(\mathcal{D}_x^0 f_i^k + \mathcal{D}_x^0 f_i^{k+1}\right) = \frac{1}{4h}\left(f_{i+1}^k - f_{i-1}^k + f_{i+1}^{k+1} - f_{i-1}^{k+1}\right) \quad . \tag{5}$$

III. Spatial Discretisation of Second Order. Finally we have to approximate the second order spatial derivative of the displacement function. As this choice is not crucial we propose a simple central approximation

$$(u_{xx})_i := \mathcal{D}_x^- \left(\mathcal{D}_x^+ u_i\right) = \frac{1}{h^2}\left(u_{i+1} - 2u_i + u_{i-1}\right) \quad . \tag{6}$$

Why the Discretisation of f_x Matters. To show that an appropriate choice of $(f_x)_i^k$ is crucial for computing reasonable displacements u, we conduct a small experiment: Consider the two frames of a signal sequence in Fig. 1 (a). Here, the signal is displaced by one position to the right in its middle part and stays unchanged otherwise, which is also indicated in the ground truth displacement in Fig. 1 (b). Note that this example comprises smooth as well as discontinuous signal and displacement regions which make it rather indicative.

In Fig. 1 (c)–(e) we depict computed displacements using different discretisations for f_x. The displacements were obtained as the solution of a linear system of equations that arises from the discretised Euler-Lagrange equation (2). As the system matrix is tri-diagonal, it can directly be solved via the Thomas algorithm [13]. Further note that we set the smoothness weight $\alpha = 10^{-4}$, to clearly see the influence of the data term where f_x occurs.

When comparing the displacements in Fig. 1 (c)–(e), the large influence of the choice of $(f_x)_i^k$ becomes obvious: Averaged central differences only perform well in the smooth signal regions at the left and right boundaries. At discontinuities they suffer from over- and undershoots. One-sided differences perform either favourably or fail totally. Obviously, the correct orientation matters here.

When using the "correct" one-sided differences, the displacement almost coincides with the ground truth, except at one point. This is, however, not due to the numerics, but is caused by the *occlusion* at the jump in the displacement. Hence the considered point at time level k does not possess a matching point at time level $k+1$ and its displacement is undefined. In the ground truth, we assign to this point the displacement of its right neighbour.

The observed behaviour in our experiment can be explained when looking into the theory of HDEs [10, 11]. There, so called *upwind* schemes are a widely used concept where the signal derivatives are approximated by "correctly oriented" one-sided differences. The correct orientation in our case means opposite to the displacement direction, see our experiment.

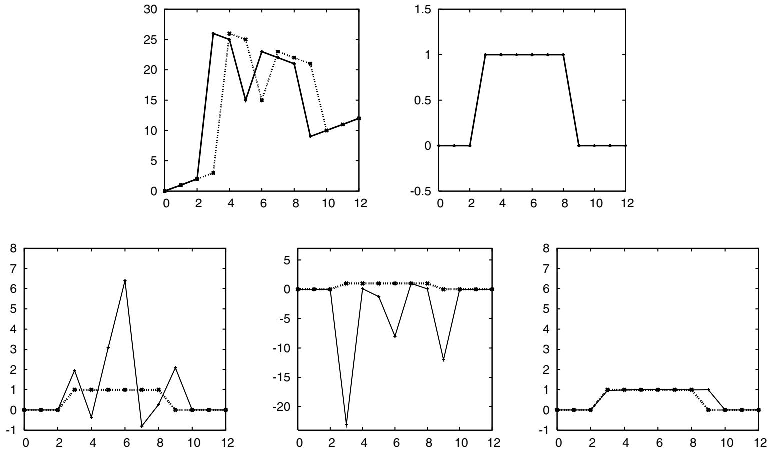

Fig. 1. Top row: (a) Signal at time k (solid) and $k+1$ (dotted). **(b)** Ground truth displacement. **Bottom row: (c)** Displacement computed using standard *averaged central* differences (solid), compared to the ground truth (dotted). **(d)** Same for one-sided *forward* differences. **(e)** Same for one-sided *backward* differences.

2.3 An Adaptive Discretisation Scheme

After explaining the outcome of our experiment with the help of hyperbolic numerics, we now adapt a successful concept from this area for our purpose.

Recall that one-sided upwind differences – that are *low-order* approximations – perform well at signal discontinuities. However, they involve a higher discretisation error than central differences that are *high-order* approximations and that perform favourably in smooth signal regions. Hence a natural idea is to combine the two strategies by using high-order approximations in smooth signal parts and low-order ones at discontinuities.

Slightly more involved techniques utilising this idea are the *high-resolution methods* [11], developed in the context of HDEs. They use a nonlinear blend of low- and high-order approximations, steered by a smoothness measure. Adapting this methodology to the variational framework will result in an *adaptive high-resolution-type (HRT)* discretisation scheme for correspondence problems, that will be presented now.

Measuring smoothness. First we discuss how to determine the smooth and discontinuous regions of a signal. Therefore we introduce a *smoothness measure*

$$\Theta_i := \Theta\left(f_i^k, f_i^{k+1}\right) := \left|\mathcal{D}_x^- f_i^k - \mathcal{D}_x^+ f_i^k\right| + \left|\mathcal{D}_x^- f_i^{k+1} - \mathcal{D}_x^+ f_i^{k+1}\right| \ , \qquad (7)$$

that is close to 0 in smooth regions where backward and forward differences of f_i^k and f_i^{k+1} are almost identical, and large at discontinuities of f_i.

Determining the Upwind Directions. Next we need to determine the appropriate upwind directions for the one-sided differences. Note that our experiment from Fig. 1 has shown that this is very crucial. We propose to compute a *predictor solution* $\tilde{u}$ whose sign determines the upwind direction. The predictor is computed using standard averaged central differences and a comparatively large smoothness weight, e.g., $\tilde{\alpha} = 1$ to cope with outliers caused by the possibly less appropriate high-order discretisation. With its help the *low-order upwind approximation* f_x^L of f_x is defined as

$$\left(f_x^L\right)_i := \begin{cases} \mathcal{D}_x^- f_i^k \ , & \text{if } \tilde{u}_i > 0 \ , \\ \mathcal{D}_x^+ f_i^k \ , & \text{if } \tilde{u}_i < 0 \ , \\ (f_x^H)_i \ , & \text{if } \ \tilde{u}_i = 0 \ , \end{cases} \tag{8}$$

where

$$\left(f_x^H\right)_i := \mathcal{D}_x^0 f_i^{k+\frac{1}{2}} \tag{9}$$

denotes the *high-order* standard approximation of f_x using averaged central differences. Revisiting the experiment from Fig. 1, we realise that this definition agrees with the results obtained there.

The High-Resolution-Type (HRT) Discretisation Scheme. Now we have everything at hand to define the adaptive HRT discretisation scheme as

$$(f_x)_i^k := \left(f_x^L\right)_i + \Phi\left(\Theta_i\right)\left[\left(f_x^H\right)_i - \left(f_x^L\right)_i\right] \ , \tag{10}$$

using a *blending function* $\Phi(\Theta_i)$. It is close to 1 in smooth signal regions (indicated by Θ_i), yielding a high-order approximation there. At discontinuities it is close to 0 which leads to a low-order approximation that is better suited there.

For the actual choice of $\Phi(\Theta_i)$ we propose

$$\Phi(\Theta_i) := \begin{cases} 1 - \frac{\Theta_i}{T} \ , & \text{if } 0 \leq \Theta_i < T \ , \\ 0 \ , & \text{else} \ , \end{cases} \tag{11}$$

using a threshold parameter $T > 0$. Note that for $T \to 0$ we obtain the upwind scheme and for $T \to \infty$ one falls back to a standard scheme.

Applying the HRT scheme to the signal sequence from Fig. 1 gives the same result as with the appropriate upwind scheme, hence we omit an additional figure. However, for more challenging stereo and optic flow problems that we discuss in Sect. 3 and 4, the blending of the HRT scheme will give results superior to a pure upwind scheme.

3 Integration into Variational Stereo Approaches

In this section we integrate our adaptive HRT discretisation scheme into a recent variational stereo approach by Slesareva et al. [6]. We restrict ourselves to the *rectified* scenario where displacements can only occur in horizontal direction and thus one has to solve a 1-D correspondence problem for each image row. However, it makes sense to couple those via a 2-D smoothness assumption, as will be described now.

3.1 Variational Stereo

We consider the image pair $f_l(\mathbf{x}) \equiv f(\mathbf{x}, t)$ and $f_r(\mathbf{x}) \equiv f(\mathbf{x}, t+1)$ denoting the left and right view of a static scene, respectively. Here, $\mathbf{x} := (x, y)^\top$ denotes the location within a rectangular image domain $\Omega_2 \subset \mathbb{R}^2$. Further assume that the images are presmoothed by a Gaussian convolution of standard deviation σ. The unknown scalar-valued *disparity* is given by the absolute value of u which can be written as $\mathbf{u} := (u, 0)^\top$ in the rectified case.

In accordance to [6], the disparity is found by minimising the energy

$$E(\mathbf{u}) = \int_{\Omega_2} [M(\mathbf{u}) + \alpha\, V(\mathbf{u})] \;\mathrm{d}\mathbf{x} \ . \tag{12}$$

The *data term*

$$M(\mathbf{u}) = \Psi_M\Big(|f_r(\mathbf{x}{+}\mathbf{u}) - f_l(\mathbf{x})|^2 + \gamma\, |\nabla f_r(\mathbf{x}{+}\mathbf{u}) - \nabla f_l(\mathbf{x})|^2\Big) \ , \tag{13}$$

where $\nabla := (\partial_x, \partial_y)^\top$ denotes the spatial gradient operator, combines the brightness and gradient constancy assumption weighted by $\gamma > 0$. The latter makes the method more robust under illumination changes. To cope with outliers caused by noise or occlusions, a robust penaliser function $\Psi_M(s^2) := \sqrt{s^2 + \varepsilon^2}$ using a small regularisation parameter $\varepsilon > 0$ is employed that results in modified L^1 penalisation. As will be described below, the linearisation of the data term is postponed to the minimisation phase to allow for a correct handling of large displacements.

The *smoothness term*

$$V(\mathbf{u}) = \Psi_V(|\nabla u|^2) \ , \tag{14}$$

uses the same robust non-quadratic penaliser function as the data term, i.e., $\Psi_V = \Psi_M$, resulting in Total Variation regularisation [8].

Concerning the minimisation of the energy (12), we refer to [6] for the corresponding Euler-Lagrange equation. To solve it, we employ a coarse-to-fine multiscale warping approach [4] and compute on each warping level small flow increments du using the *linearised* data term

$$\Psi_M\left((f_x\, du + f_t)^2 + \gamma\left[(f_{xx}\, du + f_{xt})^2 + (f_{xy}\, du + f_{yt})^2\right]\right) \ . \tag{15}$$

Note that the discretised Euler-Lagrange equation now leads to a nonlinear system of equations. After linearisation, we obtain a large but sparse linear system, which can be solved efficiently by an iterative solver of Gauß-Seidel type [14].

3.2 The HRT Discretisation Scheme for Variational Stereo

We now adapt the HRT scheme from Sect. 2.3 to the stereo setting. First, we extend the discrete grid to a 2-D version with grid sizes h_x and h_y in x- and y-direction, respectively. The images and the disparity are then approximated by $f_l(x_i, y_j) \approx f^k_{i,j}$, $f_r(x_i, y_j) \approx f^{k+1}_{i,j}$ and $u(x_i, y_j) \approx u_{i,j}$.

I. Smoothness Measures. In the 2-D stereo case, we first of all need distinct smoothness measures Θ_x, Θ_y and Θ_{xy} for the x-, y- and xy-direction, respectively. For Θ_x we use the according expression (7) from the 1-D case and Θ_y is obtained by using y- instead of x-differences. With their help, the mixed expression is defined as $\Theta_{xy} = \Theta_x + \Theta_y$.

II. Derivative Approximations. Inspecting the linearised data term from (15), we realise that now also the *second-order derivatives* f_{xx}, f_{xt}, f_{xy} and f_{yt} need to be discretised.

Due to space limitations we will exemplify our approach for f_{xy}. The other derivatives are than approximated accordingly. Note that given the two signals $f^k_{i,j}$ and $f^{k+1}_{i,j}$, the time derivative f_t is always approximated as in (3).

We start with the *high-order* approximation of $f_{xy} = \partial_x f_y$. This translates to the finite difference case as

$$(f^H_{xy})^k_{i,j} = \mathcal{D}^0_x\left(\mathcal{D}^0_y f^{k+\frac{1}{2}}_{i,j}\right) = \frac{1}{2}\Big[\mathcal{D}^0_x\left(\mathcal{D}^0_y f^k_{i,j}\right) + \mathcal{D}^0_x\left(\mathcal{D}^0_y f^{k+1}_{i,j}\right)\Big] \tag{16}$$

$$= \frac{1}{4h_y}\left[\left(\mathcal{D}^0_x\left(f^k_{i,j+1} - f^k_{i,j-1}\right)\right) + \left(\mathcal{D}^0_x\left(f^{k+1}_{i,j+1} - f^{k+1}_{i,j-1}\right)\right)\right] \tag{17}$$

$$\begin{aligned} = \frac{1}{8h_xh_y}\Big[& f^k_{i+1,j+1} - f^k_{i+1,j-1} - \left(f^k_{i-1,j+1} - f^k_{i-1,j-1}\right) \\ & + f^{k+1}_{i+1,j+1} - f^{k+1}_{i+1,j-1} - \left(f^{k+1}_{i-1,j+1} - f^{k+1}_{i-1,j-1}\right)\Big] \ . \end{aligned} \tag{18}$$

Note that for f_{xx} we employ the central discretisation in accordance to (6).

In the *low-order* case we use the upwind discretisation of $(f_x)^k_{i,j}$, steered by the predictor $\tilde{u}$. For the y-derivative we employ the averaged central difference approximation as in the rectified scenario, the displacement in y-direction is always zero. Thus we obtain for $\tilde{u} > 0$:

$$(f^L_{xy})^k_{i,j} = \mathcal{D}^-_x\left(\mathcal{D}^0_y f^k_{i,j}\right) = \frac{1}{2h_xh_y}\left(f^k_{i,j+1} - f^k_{i,j-1} - \left(f^k_{i-1,j+1} - f^k_{i-1,j-1}\right)\right) \ , \tag{19}$$

and a corresponding expression for $\tilde{u} < 0$. Note that we do not need a larger smoothness weight $\tilde{\alpha}$ to compute $\tilde{u}$ in this case since an appropriate α for usual stereo pairs will be large enough.

3.3 Experiments for Variational Stereo

We now show results for disparity computations using the approach of Slesareva et al. [6] with different derivative approximations.

We use greyscale versions of the stereo image data from the Middlebury University [15][1]. To measure the quality of estimated disparities compared to the given ground truth disparities, we employ the *bad pixel error (BPE)* measure [15]. As fixed parameters we set $\varepsilon = 10^{-3}$ and $T = 1$. In the stereo case we set $\sigma = 0.5$ and for the optic flow experiments in Sect. 4 we set $\sigma = 0.8$.

[1] Available under `http://vision.middlebury.edu/stereo`

In Fig. 2, the results for the *Plastic* pair are depicted. Considering the bad pixel maps in Fig. 2 (b)–(c), we see that the HRT scheme improves the results in the vicinity of image discontinuities and at the boundaries. Those areas are marked grey in the error maps. Note that the artefacts in Fig. 2 (f) are again caused by occlusions. The improvement also becomes visible in the BPE measures that are summarised in Table 1 that also lists other Middlebury pairs and parameter settings. Also error measures for a pure upwind scheme are given there. Comparing them to the HRT scheme shows that the blending of the latter scheme also pays off in terms of quality measures.

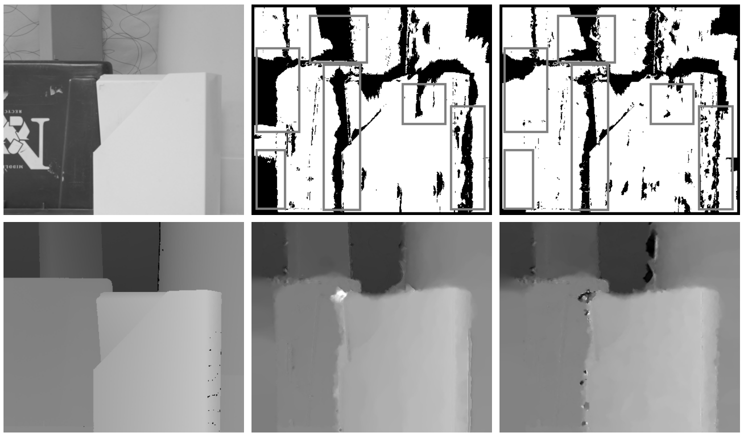

Fig. 2. Top row: (a) Left image of the *Plastic* pair. **(b)** Bad pixels for approach with a standard derivative approximation (bad pixels are coloured black). **(c)** Same for the HRT scheme. **Bottom row: (d)** Ground truth disparity. **(e)** Disparity for approach with a standard derivative approximation. **(f)** Same for the HRT scheme.

4 Extension to Variational Optic Flow

Having presented how to employ the adaptive HRT discretisation scheme for stereo, its extension to the optic flow case is more or less straightforward.

For optic flow we consider a presmoothed image sequence $f(\mathbf{x}, t)$ and want to compute a *flow field* $\mathbf{w} := (u, v)^\top$, where u and v give the displacements in x- and y-direction, respectively. Using the method of Brox et al. [4] that was the basis for the stereo approach of Slesareva et al. [6], we compute $\mathbf{w}$ as the minimiser of an energy functional similar to the one from (12).

One difference concerning the HRT scheme is that we now also have to approximate f_y and f_{yy}. This, however, works accordingly to the stereo case.

More problematic are the low-order upwind approximations of f_{xy}, as they now depend on a predictor $\tilde{\mathbf{w}} = (\tilde{u}, \tilde{v})^\top$. Hence we need to do an extensive case distinction taking into account all possible combinations of the signs of $\tilde{u}$ and $\tilde{v}$. For example, let $\tilde{u} > 0$ and $\tilde{v} < 0$ then

Table 1. BPE measures and parameters for stereo experiments

Image Pair	Derivative Approximation	Parameters	BPE
Plastic	standard	$\alpha = 5.5, \gamma = 190.0$	25.85
	upwind	$\alpha = 5.5, \gamma = 190.0$	21.35
	HRT scheme	$\alpha = 5.5, \gamma = 190.0$	18.85
Teddy	standard	$\alpha = 8.0, \gamma = 9.5$	17.45
	upwind	$\alpha = 8.0, \gamma = 9.5$	16.94
	HRT scheme	$\alpha = 8.0, \gamma = 9.5$	16.75
Venus	standard	$\alpha = 4.5, \gamma = 0.5$	3.06
	upwind	$\alpha = 4.5, \gamma = 0.5$	2.78
	HRT scheme	$\alpha = 4.5, \gamma = 0.5$	2.77

$$(f_{xy}^L)_{i,j}^k = \mathcal{D}_x^- \left(\mathcal{D}_y^+ f_{i,j}^k \right) = \frac{1}{h_x h_y} \left(f_{i,j+1}^k - f_{i,j}^k - \left(f_{i-1,j+1}^k - f_{i-1,j}^k \right) \right) \quad . \tag{20}$$

In order to show that the HRT scheme also performs favourably for optic flow, we performed experiments using the recent optic flow data sets from the Middlebury University [16][2]. In Fig. 3 we show results obtained for the *Urban3* sequence. Note that the error maps now show the magnitude of the *average angular error (AAE)* [17] measure. Inspecting them, the favourable performance of the HRT scheme in the marked regions becomes visible, which is also reflected in the AAE measures shown in Table 2. It again comprises also other Middlebury sequences, parameter settings and results for the upwind scheme. Concerning the latter, we see that also for optic flow, the HRT scheme performs better.

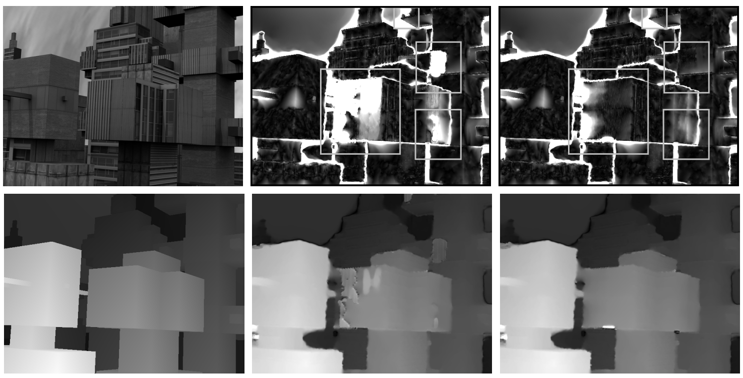

Fig. 3. Top row: (a) Frame 10 of the *Urban3* sequence. **(b)** AAE map for approach with a standard derivative approximation. **(c)** Same for the HRT scheme. **Bottom row: (d)** Flow magnitude of the ground truth. **(e)** Flow magnitude for approach with a standard derivative approximation. **(f)** Same for the HRT scheme.

[2] Available under `http://vision.middlebury.edu/flow`

Table 2. AAE measures and parameters for optic flow experiments

Image Sequence	Derivative approximation	Parameters	AAE
Urban3	standard	$\alpha = 4.5, \gamma = 4.0$	5.71
	upwind	$\alpha = 4.5, \gamma = 4.0$	4.58
	HRT scheme	$\alpha = 4.5, \gamma = 4.0$	4.11
RubberWhale	standard	$\alpha = 50.0, \gamma = 50.0$	4.72
	upwind	$\alpha = 50.0, \gamma = 50.0$	4.73
	HRT scheme	$\alpha = 50.0, \gamma = 50.0$	4.34
Dimetrodon	standard	$\alpha = 7.0, \gamma = 10.0$	1.94
	upwind	$\alpha = 7.0, \gamma = 10.0$	3.06
	HRT scheme	$\alpha = 7.0, \gamma = 10.0$	1.88

5 Conclusions and Outlook

In this paper we have presented a sophisticated numerical scheme for the approximation of spatial image derivatives in variational approaches to correspondence problems. Our experiments demonstrated that such a scheme allows to tangibly improve the quality of results, which has in more than 20 years of research in this field only been experienced by model refinements. We hence conjecture that the numerics can be a fruitful alternative starting point for further advances.

This finding is no surprise for people acquainted with the theory of HDEs where sophisticated numerical schemes have been thoroughly investigated. In this paper we have seen that HDEs and variational approaches share some structural similarities. However, we were the first to utilise this similarity for developing a well-engineered numerical scheme for variational approaches.

We want to stress that the adaptive discretisation scheme developed within this paper is for sure not the only lucrative technique that can be adapted from the field of HDEs. Our current research is thus concerned with exploring further directions that may lead to better numerical schemes for variational approaches to correspondence problems.

Acknowledgement

Henning Zimmer gratefully acknowledges funding by the International Max-Planck Research School (IMPRS).

References

1. Horn, B., Schunck, B.: Determining optical flow. Artificial Intelligence 17, 185–203 (1981)
2. Alvarez, L., Deriche, R., Papadopoulo, T., Sanchez, J.: Symmetrical dense optical flow estimation with occlusions detection. International Journal of Computer Vision 75(3), 371–385 (2007)

3. Ben-Ari, R., Sochen, N.: Variational stereo vision with sharp discontinuities and occlusion handling. In: Proc. 2007 IEEE International Conference on Computer Vision, Rio de Janeiro, Brazil, pp. 1–7. IEEE Computer Society Press, Los Alamitos (2007)
4. Brox, T., Bruhn, A., Papenberg, N., Weickert, J.: High accuracy optical flow estimation based on a theory for warping. In: Pajdla, T., Matas, J. (eds.) ECCV 2004. LNCS, vol. 3024, pp. 25–36. Springer, Heidelberg (2004)
5. Nir, T., Bruckstein, A.M., Kimmel, R.: Over-parameterized variational optical flow. International Journal of Computer Vision 76(2), 205–216 (2008)
6. Slesareva, N., Bruhn, A., Weickert, J.: Optic flow goes stereo: A variational method for estimating discontinuity-preserving dense disparity maps. In: Kropatsch, W., Sablatnig, R., Hanbury, A. (eds.) DAGM 2005. LNCS, vol. 3663, pp. 33–40. Springer, Heidelberg (2005)
7. Zimmer, H., Bruhn, A., Valgaerts, L., Breuß, M., Weickert, J., Rosenhahn, B., Seidel, H.P.: PDE-based anisotropic disparity-driven stereo vision. In: Deussen, O., Keim, D., Saupe, D. (eds.) Proceedings of Vision, Modeling, and Visualization (VMV) 2008, pp. 263–272. AKA, Heidelberg (2008)
8. Rudin, L.I., Osher, S., Fatemi, E.: Nonlinear total variation based noise removal algorithms. Physica D 60, 259–268 (1992)
9. Marquina, A., Osher, S.: Explicit algorithms for a new time dependent model based on level set motion for nonlinear deblurring and noise removal. SIAM Journal on Scientific Computing 22(2), 387–405 (2000)
10. LeVeque, R.J.: Numerical Methods for Conservation Laws. Birkhäuser, Basel (1992)
11. LeVeque, R.J.: Finite Volume Methods for Hyperbolic Problems. Cambridge University Press, Cambridge (2002)
12. Morton, K.W., Mayers, L.M.: Numerical Solution of Partial Differential Equations. Cambridge University Press, Cambridge (1994)
13. Thomas, L.H.: Elliptic problems in linear difference equations over a network. Technical report, Watson Scientific Computing Laboratory. Columbia University, New York (1949)
14. Saad, Y.: Iterative Methods for Sparse Linear Systems, 2nd edn. SIAM, Philadelphia (2003)
15. Scharstein, D., Szeliski, R.: A taxonomy and evaluation of dense two-frame stereo correspondence algorithms. International Journal of Computer Vision 47(1-3), 7–42 (2002)
16. Baker, S., Roth, S., Scharstein, D., Black, M., Lewis, J., Szeliski, R.: A database and evaluation methodology for optical flow. In: Proc. 2007 IEEE International Conference on Computer Vision, Rio de Janeiro, Brazil, pp. 1–8. IEEE Computer Society Press, Los Alamitos (2007)
17. Barron, J.L., Fleet, D.J., Beauchemin, S.S.: Performance of optical flow techniques. International Journal of Computer Vision 12(1), 43–77 (1994)